SEM-Newmark sliding mass analysis for regional coseismic landslide hazard evaluation: a case study of the 2016 Kumamoto earthquake

Zhengwei Chen[1] and Gang Wang[1*]

[1] Hong Kong University of Science and Technology, Hong Kong
Corresponding author: gwang@ust.hk

Abstract. Coseismic landslides have been observed to cause severe damage during many historic earthquakes. Numerical simulation of fault rupture process, wave propagation and triggering of landslides considering realistic topography and geological conditions helps identify the key factors in the landslide triggering and evaluate the potential slope instability in seismically active areas.
In this study, a physics-based regional coseismic landslide evaluation framework is constructed by integrating the flexible sliding analysis into spectral element model (SEM). The framework combines advantages of SEM model for its capability of simulating complex 3D large-scale wave propagation and a flexible mass sliding analysis for capturing local soil response in coseismic slope stability evaluation. Besides, equivalent linear method is implemented to incorporate the effect of soil nonlinearity.
The developed model is adopted to simulate the landslides in the Aso Volcano area triggered by the 2016 Kumamoto earthquake. Realistic digital elevation model, site conditions and fault rupture model of simulated region (51km × 43km) are used in the simulation. The resulting sliding response is compared with the inventory of the triggered landslides to validate the proposed model.

Keywords: Coseismic landslide, Spectral element method, Flexible sliding analysis, Equivalent linear model, 2016 Kumamoto earthquake.

1 Introduction

Earthquake-induced landslides have caused catastrophic damage to human society. For example, the 1994 Northridge earthquake caused more than 57 deaths and over 9000 injuries, and more than 82000 residential and commercial units were damaged. It is important to estimate the location and severity of triggered landslides given earthquake and geologic conditions. In the seismic hazard evaluation procedure, prediction of the permanent sliding displacement is commonly conducted, and it is crucial for the design of infrastructure and protection of human lives. There are many factors affecting seismic response of natural terrains, such as topography, site condition, soil properties, and characteristics of earthquake motions. These factors can significantly affect regional

wave propagation and local ground-motion amplification, which need to be considered in the prediction of coseismic landslides.

A typically used method for the sliding displacement calculation is Newmark sliding block method [1]. It models landslide as a rigid block sliding on an inclined slope; A yield acceleration is determined to represent the resistance of the block against sliding. The sliding displacement is calculated by double integrating the difference between ground-motion acceleration and the yield acceleration in the time domain, until the sliding velocity becomes zero. Many studies have extended this method to flexible sliding masses by accounting for the response of soil layers [2-5], and many regressed predictive equations have been developed [6-9]. However, these studies are based on 1D local site response analysis without considering regional wave propagation and 3D topographic effects.

In this study, a physics-based regional coseismic landslide evaluation framework is constructed by integrating the rigid/flexible sliding analysis into wave propagation simulation. The wave propagation simulation is conducted using spectral element method (SEM) that is capable of simulating complex large-scale 3D wave propagation. Its local site response is used in the sliding analysis to calculate potential sliding displacement. Besides, an equivalent linear method is implemented to incorporate the effects of soil nonlinearity. The developed model is applied to simulate the coseismic landslides in the Aso Volcano area triggered by the 2016 Kumamoto earthquake.

2 Development of regional coseismic landslide evaluation framework

Fig. 1 shows the overall framework of the proposed model. We use the realistic digital elevation data to construct a 3D SEM model for a regional scale wave propagation simulation. During the simulation, shear stress acting on the sliding interface is used to drive the sliding mass at each time step.

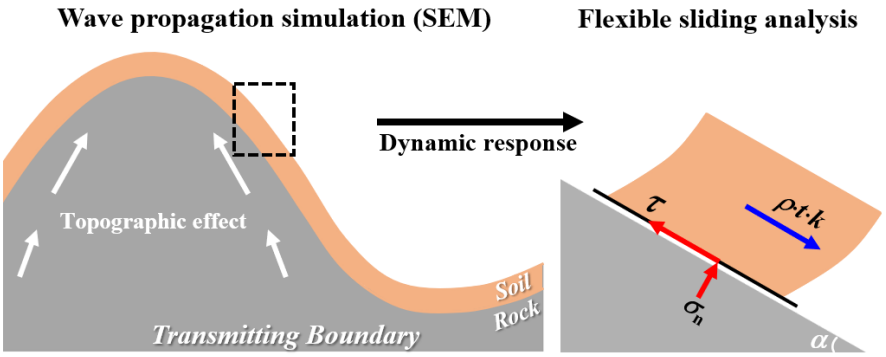

Fig. 1. Illustration for regional coseismic landslide analysis framework

2.1 Wave propagation simulation

For the regional scale wave propagation simulation, the Spectral Element Method (SEM) is adopted to model the complex topography and site conditions. SEM is efficient and accurate for wave propagation simulation [10]. Using high-order interpolation functions, the SEM is capable of capturing a wavelength within one mesh. To improve the computational efficiency, we used a graded mesh in soil and rock, such that the numerical model is accurate to simulate a wave frequency up to 5 Hz.

2.2 Implementation of equivalent linear model

Accurate modeling of nonlinear soil behavior is important for the seismic hazard assessment, where variation of soil stiffness and energy dissipation due to soil nonlinearity should be considered [11]. The equivalent-linear method (ELM) is commonly used to approximate the soil nonlinearity in site response analysis [12]. Fig. 2a shows the implementation of ELM in SEM by iteratively adjusting soil properties to reach a strain-compatible modulus (G) and damping ratio (λ) in each soil element. Firstly, the small-strain soil modulus and damping are chosen, and a new strain field is derived after the wave propagation analysis; Then, G and λ are updated according to the new strain field, and this procedure is repeated until the relative error of the maximum shear strain (γ_{max}) is less than 2%; finally, the strain-compatible soil properties are achieved and the dynamic response can be applied in the sliding analysis procedure. Note that the effective strain is adopted for the updating of soil modulus and damping, which is typically 65% of the maximum strain.

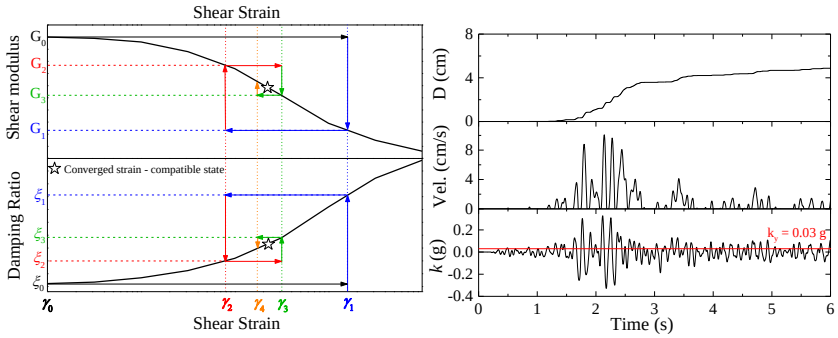

Fig. 2. (a) Iteration procedure of ELM (b) Newmark analysis algorithm in SEM model

2.3 Flexible sliding analysis

The Newmark-type sliding analysis method is commonly used in the evaluation of natural slopes or earthquake-induced landslides, because it provides a simple index of the seismic slope performance. The calculation requires two parameters: acceleration-time history (k) representing the driving force, and a yield acceleration (k_y) indicating resistance on the sliding interface. In this study, k is determined by the shear stress on

sliding interface divided by the mass of the sliding column, which also represents the averaged acceleration within the soil mass (Fig. 1). As illustrated in Fig. 2b, sliding displacement (D) is accumulated by double integration of (k - k_y) until the sliding velocity becomes zero.

The sliding calculation requires a pre-defined sliding direction, and it is assumed along the dip direction of the slope. The aspect and slope angles can be calculated using the digital elevation data of the simulated region. Then, shear stress τ along the sliding direction (also called tangential direction) can be obtained by projection of the stress tensor. Accordingly, the seismic coefficient k, can be derived as follow:

$$k = \frac{\tau}{\rho t} \tag{1}$$

where ρ is the density of the soil; t is the thickness of the sliding layer; α is the slope angle.

Conventional Newmark sliding block method represents the shear resistance by the yield acceleration k_y, which is a function of static factor of safety (FS) and slope angle (α) as follow [7]:

$$k_y = (FS - 1) \cdot \mathrm{g} \cdot \sin\alpha \tag{2}$$

Using a limit-equilibrium model of an infinite slope, FS is derived as follow:

$$FS = \frac{c'}{\rho g t \sin\alpha} + \frac{\tan\varphi'}{\tan\alpha} - \frac{m\rho_w \tan\varphi'}{\rho \tan\alpha} \tag{3}$$

where c' and φ' are the effective cohesion and friction angle; ρ and ρ_w are soil and water densities; t is soil thickness in the slope-normal direction; m is the proportion of soil that is submerged, which in this study is set to zero. By introducing the Eq. (3) to Eq. (2), the k_y can be derived as:

$$k_y = \frac{c'}{\rho t} + (\tan\varphi' \cos\alpha - \frac{m\rho_w \tan\varphi' \cos\alpha}{\rho} - \sin\alpha) \cdot g \tag{4}$$

3 Coseismic landslides in Aso volcano area triggered by the 2016 Kumamoto earthquake

On April 14, 2016, an M_w 7.0 earthquake occurred in Kumamoto and Oita Prefectures, central Kyushu, Japan. More than 100 people were killed, 2000 were injured and 38000 houses were destroyed due to surface rupture, strong ground motion and landslides [13]. This earthquake caused more than 3000 landslides with a sliding area of around 7 km^2 [14]. Most of landslides triggered by this event were shallow, disrupted failures with a few flow-type slides and large rock/soil avalanches. The most impressive characteristic of the landslides is that they were highly concentrated around the Aso volcano area.

In this study, the SEM model is constructed to reproduce the full process of this earthquake, including the earthquake rupture process, wave propagation and induced coseismic landslides in a study area of 51km × 43km around the Aso volcano, as illustrated in Fig. 3. The highest elevation is more than 1.5 km above the sea level atop Aso caldera.

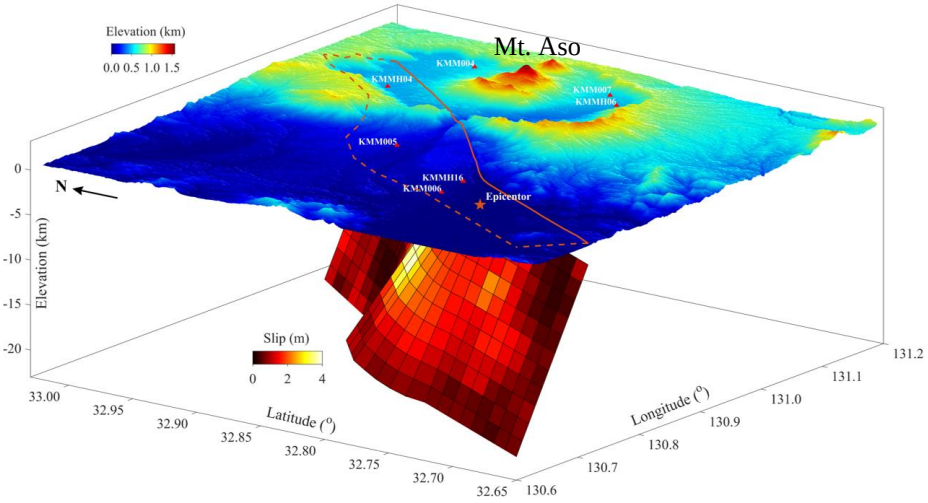

Fig. 3. Illustration of the Aso volcano area and underlying rupture in the SEM model.

3.1 Source rupture process of the 2016 Kumamoto earthquake

Through multiple-time-window linear waveform inversion, the rupture process of the M_w 7.0 main event is derived [13]. As shown in Fig. 4a, the fault can be modelled as a curved fault plane divided into 28 subareas along the strike direction and 12 subareas along the dip direction, each with a size of approximately 2 km × 2 km. Fig. 4b shows total slip in each subarea. Large fault rupture mainly occurred in three regions, including the Kumamoto region, the region north of Mt. Aso, and the Oita region. The surface rupture has extended approximately 30 km and almost reached the caldera of Mt. Aso.

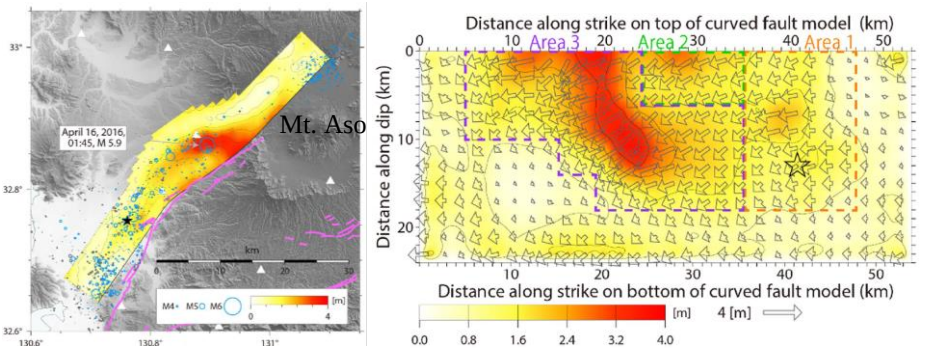

(a) (b)

Fig. 4. (a) Map projection of the total slip distribution for the main even (epicenter is the star); (b) Planar projection of the total slip distribution (the vectors denote the direction and the slip amount on the hanging wall side) [13].

The rupture process is represented by a number of point sources in SEM, each source has its own time history referring to the given slip velocity time functions [13]. Moment tensor of each subarea is calculated with its final slip, slip, dip and rake directions.

3.2 Velocity structure and strength parameters

The velocity structure adopted in this study refers to the 3D subsurface structure model of this region [15] and soil condition data explored at K-net and KiK-net stations d provided by National Research Institute for Earth Science and Disaster Resilience (NIED) of Japan.

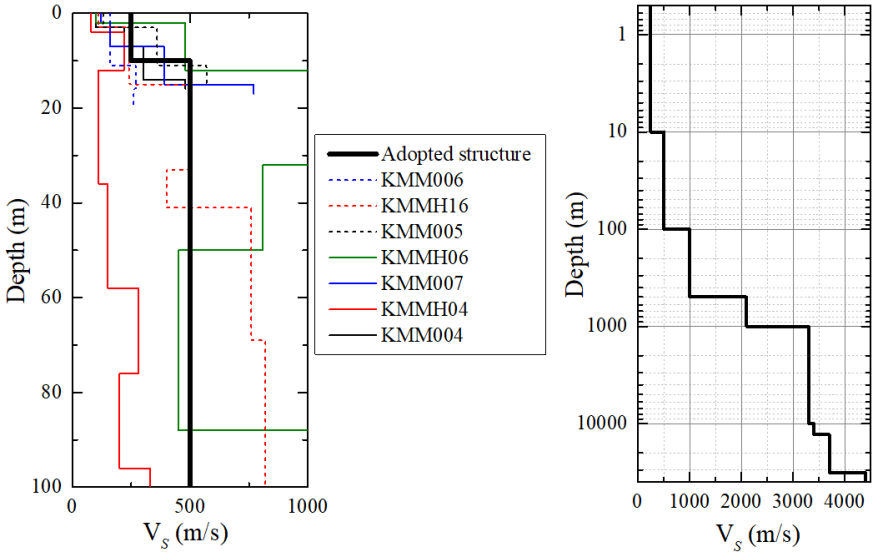

Fig. 5. Velocity structure within (a) shallow layer and (b) deep layer

Information on the soil strength parameters within the Aso volcano is very limited, as not many laboratory or in-situ tests have been conducted. The strength constants obtained by a simple test using a soil strength probe gives a friction angle of approximately 30° and cohesion of 3.5 kPa for the pumice around this area, while these two parameters are 2.0 kPa and 15° for volcanic ash [16]. The vane cone shear test was performed by [17] on a site in the Sanno-Tanigawa area in the southwest part of Mt. Eboshidake and obtained a cohesion between 4 and 10 kPa and a friction angle within 20 to 40 degrees. They also showed that for pumice in the Takanodai area, the cohesion is in the range of 5 to 15 kPa and friction angle of 25 to 45 degrees. A back calculation for strength parameters around this area using Newmark method was conducted to fit the realistic triggered landslides in [18], and a detailed summary for strength parameters for different geologic classifications is given. In this study, we set strength constants by referring to available experimental data, and for those not available we adopted the inferred values by [18]. Besides, sliding depths of 3 m around the central cones and 10 m around

the caldera edge are identified as potential sliding depth, where shear stresses are recorded to calculate the seismic coefficient *k*.

3.3 Wave propagation and ground motion distribution

Fig. 6 illustrates the ground velocity in the East-West direction at different times. In this simulation, the fault rupture was triggered at 0 sec at the hypocenter located around 13 km in depth. It took less than 6 seconds for the wave to reach the ground, and then radiated outwards (see Fig. 6a). The rupture propagated to the northeast direction and the strong-motion directivity effect can be observed, as demonstrated by strong velocity as great as 1.5 m/s in northeast area (see Fig. 6b). The whole rupture process lasted around 16 seconds, while the entire simulation lasted 30 seconds until the seismic wave field propagated out of the computational domain.

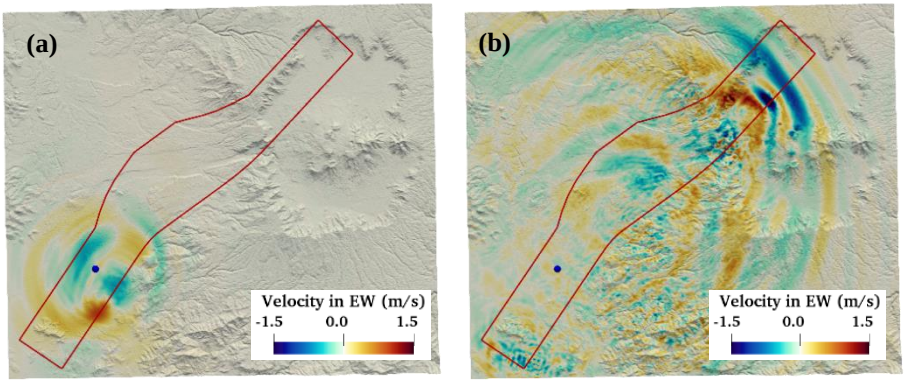

Fig. 6. Ground velocity in the East-West direction at (a) t = 6 sec and (b) t = 14 sec

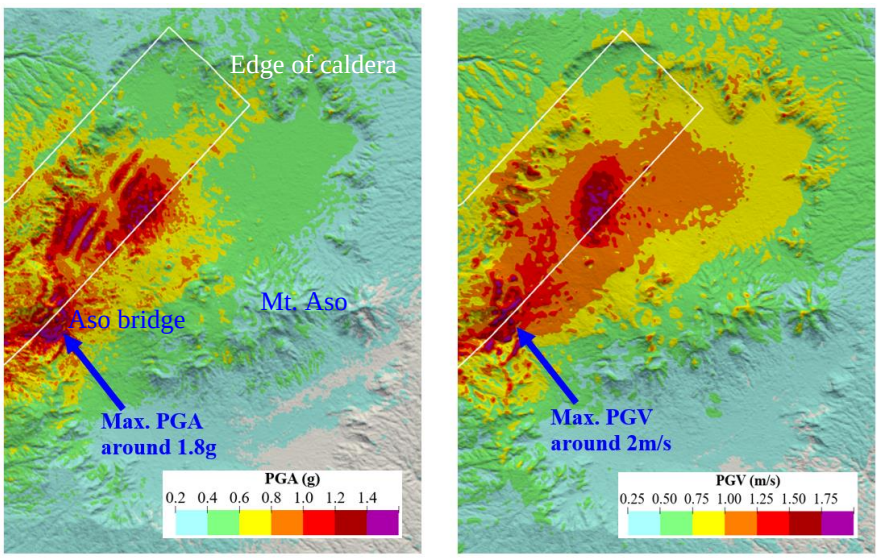

Fig. 7. PGA and PGV maps around Aso Volcano

The PGA and PGV shakemaps around Aso volcano are shown in Fig. 7. It can be seen that large PGA and PGV are concentrated on the projected area of the fault plane, i.e., the hanging wall side of the fault plane. The strong motions in this region are mainly contributed by the directivity effect and larger rupture slip (as shown in Fig. 4). Obvious topographic amplification was also observed around the edge of the Aso caldera, and we simulated a significantly large PGA of 1.8 g in the Aso bridge area due to this local topographic effect [19-20]. Similarly, we simulated a PGV as large as 2 m/s in this location. The central cones of Aso caldera experienced relatively moderate ground motions, with PGA values between 0.2 g and 0.6 g and PGV values in the range of 0.25 m/s to 0.75 m/s. As the rupture distance increases, the peak ground motion decreases gradually. The distribution of these ground motions is closely related to the triggered landslide pattern, as will be discussed in the following part.

3.4 Predicted landslide and its comparison with inventory

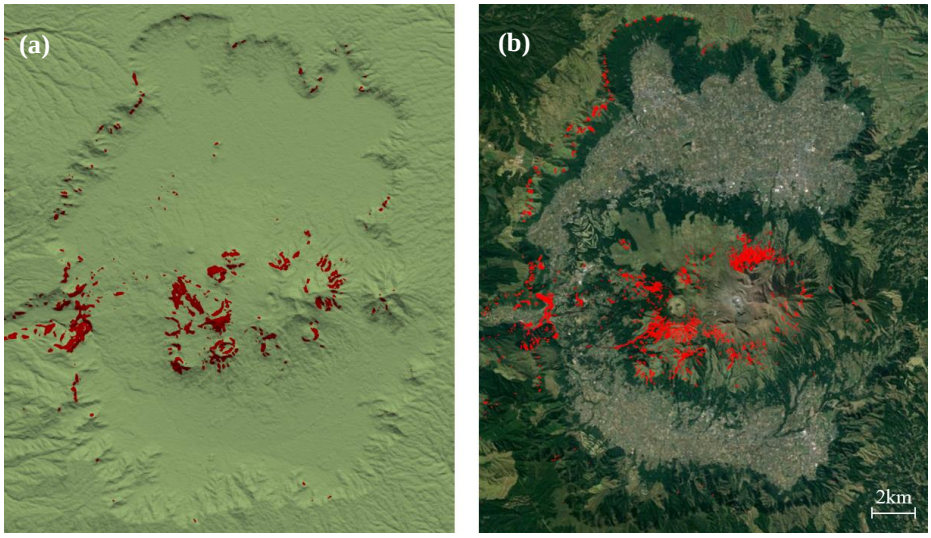

Fig. 8. Comparison of coseismic landslides (a) by SEM-Newmark prediction and (b) inventory data (compiled from [21] and [22])

The SEM-Newmark sliding analysis method evaluates the difference between the seismic coefficient k (calculated from Eq. 1) and sliding resistance k_y (calculated from Eq. 4), and it leads to sliding episodes and accumulation of permanent sliding displacements in the downslope direction. In this study, the field of sliding resistance k_y was pre-calculated using the estimated soil strengths. Then, during the SEM simulation of wave propagation, the driving force (shear stress along the sliding interface) at each time step was recorded to calculate the relative sliding displacement at each location. Sliding was considered to occur when the sliding displacement was greater than 15cm.

Finally, a sliding map was derived based on the SEM-Newmark prediction, as shown in Fig. 8a.

The landslide inventory data is used to verify our prediction based on the landslide survey conducted by the Forest Agency of the Ministry of Agriculture, Forestry, and Fisheries, Japan [21]. They carried out high-density aerial laser measurements to identify the occurrence of landslides and cracks in the slope after the 2016 Kumamoto earthquake. As reported, the inventory map was precise after analyzing the detailed topographic map and orthorectified aerial photographs. Sliding data in some areas inside the Aso caldera are missing, and we refer to another investigation conducted by NIED [22]. These two inventories complemented each other and provided the final landslide inventory map adopted in this study (cf. Fig. 8b).

Overall, our predicted landslide distribution generally matches the inventory data. It can be found that landslides were mainly concentrated on central cones and the western edge of the caldera. A great amount of pumice with low cohesion and friction angle were located around the central cones, leading to significant amount of landslides in that area due to weak soil strength. Note that the ground motions within this region are quite strong, with PGA around 0.5 g and PGV around 75cm/s. The intensive ground motions along the western edge of the caldera also lead to great amount of landslides. One of the most notable destroyed the Aso bridge [14]. In addition, the northwestern edge of the caldera also suffered severe damage.

Fig. 9 illustrates the distribution of slope angles and the percentage of landslides by statistical analysis using grid cells of 5 m×5 m. Note that the inventory data includes both the sliding sources and deposits, while the Newmark method only evaluates the potential sliding source based on a threshold value. In this study, we identify the sliding sources as the upper half of the sliding mass in the inventory based on common practice. Fig. 9 shows that around 38% of the landslide source occurred on slope with angles of 10 - 20°, and 32% occurred on slope angles of 20 - 30°. The corresponding percentages of the predicted landslides by Newmark analysis are also reported for comparison using different threshold values of sliding displacements.

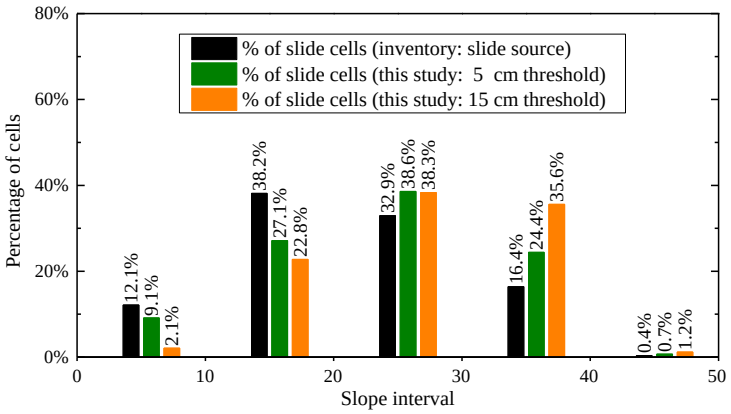

Fig. 9. Distribution of slope angle for landslide cells

Finally, we evaluate the accuracy of the SEM-Newmark prediction by one-to-one comparison of the predicted and measured landslides using the 5 m×5 m grid cells. If a threshold sliding displacement of 15 cm is adopted, the SEM-Newmark model can capture 37.4% of the sliding sources from the inventory, and the model over-predicted the landslide area by a factor of 4.6. If a more conservative threshold of 5 cm is adopted, the SEM-Newmark model can capture up to 50.5% of the sliding sources, however, the over-prediction ratio increases to 7.7.

4 Summary and discussion

In this study, a computational framework is proposed by integrating 3D physics-based wave propagation simulation with the Newmark-type sliding mass analysis for a regional evaluation of coseismic landslides. The model is examined by simulating wave propagation and coseismic landslides in Kumamoto Prefecture during the 2016 Kumamoto earthquake. This study is first of its kind to evaluate regional coseismic landslide (51km × 43km) considering realistic rupture process, wave propagation, topographic-site effect, and local site conditions. The rupture directivity and ground motion amplification effects are clearly observed, as demonstrated in the ground motion maps. The sliding analysis satisfactorily identifies the potential sliding areas, with prediction accuracy up to 50% (using 5 cm as threshold).

The accurate prediction of coseismic landslides is attributed to reasonable strength values adopted for various geologic classifications in this region, which helps identify areas susceptible to seismic hazards. Besides, accurate simulation of the wave propagation is also very important, because they can be significantly amplified due to local topography and altered by the pattern of fault rupture. Despite the good performance of the proposed framework, it still remains as a challenge to preciously predict all sliding areas especially for such a large region. This is because of the existence of many uncertainties and variabilities. For example, velocity structure of the domain, crucial to the wave propagation, is treat as uniformly distributed based on limited geologic data. The rupture process obtained from the waveform inversion also included many sources of uncertainties. Other factors like soil strength, material nonlinearity, sliding depth and plant root reinforcement also affect the prediction. These effects will be investigated in a future study.

Acknowledgements

The study is supported by Hong Kong Research Grants Council (Grant No. 16214220).

References

1. Newmark, N.M.: Effects of earthquakes on dams and embankments. Geotechnique 15, 139-159 (1965).
2. Seed, H.B., Martin, G.R.: The seismic coefficient in earth dam design. Journal of the Soil Mechanics and Foundations Division 92(3), 25-58 (1966).

3. Bray, J.D., Rathje, E.M.: Earthquake-induced displacements of solid-waste landfills. Journal of Geotechnical and Geoenvironmental Engineering 1243, 242-253 (1988).
4. Wang, G.: Efficiency of scalar and vector intensity measures for seismic slope displacements. Frontiers of Structural and Civil Engineering 6(1), 44-52 (2012).
5. Rathje, E.M., Antonakos, G.: A unified model for predicting earthquake-induced sliding displacements of rigid and flexible slopes. Engineering Geology 122(1-2), 51-60 (2011).
6. Saygili, G., Rathje, E.M.: Empirical Predictive Models for Earthquake-Induced Sliding Displacements of Slopes. Journal of geotechnical and geoenvironmental engineering 134(6), 790-803 (2008).
7. Jibson, R.W.: Regression models for estimating coseismic landslide displacement. Engineering geology 91(2-4): 209-218 (2007).
8. Bray, J.D., Travasarou, T.: Simplified procedure for estimating earthquake-induced deviatoric slope displacements. Journal of geotechnical and geoenvironmental engineering 1334, 381-392 (2007).
9. Watson-Lamprey, J., Abrahamson, N.: Selection of ground motion time series and limits on scaling. Soil Dynamics and Earthquake Engineering 265, 477-482 (2006).
10. Komatitsch, D., Vilotte, J.P.: The spectral element method: an efficient tool to simulate the seismic response of 2D and 3D geological structures. Bulletin of the Seismological Society of America 88(2), 368-392 (1998).
11. Kaklamanos, J., Bradley, B.A.: Critical Parameters Affecting Bias and Variability in Site-Response Analyses Using KiK-net Downhole Array Data. Bulletin of the Seismological Society of America 103(3), 1733-1749 (2013).
12. Zalachoris, G., Rathje, E.M.: Evaluation of One-Dimensional Site Response Techniques Using Borehole Arrays. Journal of Geotechnical and Geoenvironmental Engineering 141(12), 04015053 (2015).
13. Kubo, H., Suzuki, W., Aoi, S., Sekiguchi, H.: Source rupture processes of the 2016 Kumamoto, Japan, earthquakes estimated from strong-motion waveforms. Earth, Planets and Space 68(1), 1-13 (2016).
14. Xu, C., Ma, S., Tan, Z., Xie, C., Toda, S., Huang, X.: Landslides triggered by the 2016 Mj 7.3 Kumamoto, Japan, earthquake. Landslides 15(3), 551-564 (2018).
15. Fujiwara, H., Kawai, S., Aoi, S., Morikawa, N., Senna, S., Kudo, N., Ooi, M., Hao, K.X., Hayakawa, Y., Toyama, N., Matsuyama, H., Iwamoto, K., Suzuki, H., Liu, Y.: A study on subsurface structure model for deep sedimentary layers of Japan for strong-motion evaluation. In: Technical note 337, National Research Institute for Earth Science and Disaster Prevention, Tsukuba, Japan (2009).
16. Kanai, T., Asai, K., Sasaki, Y., Norimizu, S.: Evaluation of slope stability based on the soil strength probe. Proceeding of Japan Society of Engineering Geology, 169-170 (2016).
17. Fukunaga, E., Shimizu, O.: Soil layer structure and soil strength in the vicinity of the slip surface in the collapsed area of the Aso central volcano induced by the 2016 Kumamoto earthquake. Proceeding of Japan Society of Erosion Control Engineering, 676-678 (2017).
18. Shinoda, M., Miyata, Y., Kurokawa, U., Kondo, K.: Regional landslide susceptibility following the 2016 Kumamoto earthquake using back-calculated geomaterial strength parameters. Landslides 16(8), 1497-1516 (2019).
19. Huang, D., Wang, G., Du, C., Jin, F., Feng, K., Chen, Z.: An integrated SEM-Newmark model for physics-based regional coseismic landslide assessment. Soil Dynamics and Earthquake Engineering 132, 106066 (2020).
20. Chen, Z., Huang, D., Wang, G., Jin, F.: Topographic amplification on hilly terrain under oblique incident waves. In: Tournier, J.P., Bennett, T., Bibeau, J. Sustainable and Safe Dams

Around the World, ICOLD Proceedings vol. 2, pp. 2778-2786. CRC Press, Netherlands (2019).
21. Forest Agency of the Ministry of Agriculture, Forestry, and Fisheries: Report of aviation laser measurement work in the forest area (2016).
22. NIED: https://www.bosai.go.jp/mizu/dosha.html, last accessed 2021/10/30.